# 热压条件下激光深熔焊接温度场的数值模拟

熊智军， 李永强， 赵熹华， 李 民*
（吉林大学 材料科学与工程学院，长春 130022）

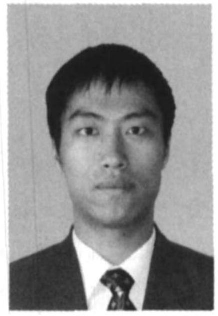

熊智军

摘 要：对铝合金 LF3Y2 搭接板进行了热压条件下激光深熔焊接。建立了该条件下的焊接热源模型，热源模型由作用在工件表面的高斯面热源和沿激光入射方向的旋转高斯体热源构成。使用该热源模型和 ANSYS 有限元分析软件对前述的试验进行了数值模拟。结果表明，热压使激光在高速焊接时依然有足够的熔深和熔宽；试件表面的等温线呈椭圆形，在移动热源前方温度梯度大，后方温度梯度小；计算所得的熔池截面成形与工艺试验结果吻合良好，验证了该热源模型的合理性。

关键词：激光深熔焊接；热源模型；数值模拟；温度场
中图分类号：TG456.7 文献标识码：A 文章编号：0253－360X(2007)08－041－04

## 0 序 言

铝合金由于其比强度高、耐腐蚀、易加工成形及美观耐用等优点，广泛应用于航空航天、汽车制造等领域。激光焊是 21 世纪最具发展潜力的焊接方法，但由于铝合金的高反射率、苛刻的焊前预处理要求及焊缝中易产生气孔、裂纹缺陷等，极大地限制了其在工程的实际应用[1－5]。激光束－电阻缝焊（LB－RSW）是一种崭新的复合焊接方法[6]，利用数值模拟技术认识其焊接热过程，无疑对铝合金 LB－RSW 焊接温度场分布规律，减少焊接缺陷，控制焊缝成形，实现质量监控等具有重要的理论意义和实际应用价值。热压条件下的搭接铝合金板激光深熔焊接是 LB－RSW 复合焊接的重要基础研究内容，它是优化该方法工艺和系统设计的重要依据。

## 1 试样制备

试样材料为铝合金 LF3Y2，规格为 100 mm× 100 mm× 1.4 mm 的两板搭接组成，焊前表面处理，即表面除油（丙酮）→打磨（240 号砂纸）→刷光（ϕ0.15 mm不锈钢丝刷）。试样经 FZ－1602 电阻缝焊机热压焊后，在 DC－030 $CO_2$ 激光焊机上进行焊接。所获得的 LB－RSW 试样焊接接头外观照片见图 1，金相照片见图 2。

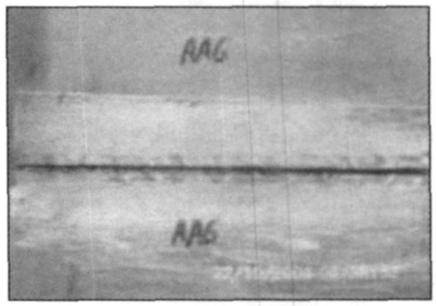


图 1 LF3Y2 铝合金试样焊接接头外观

Fig 1 Appearance of welded joint sample of aluminum alloy LF3Y2

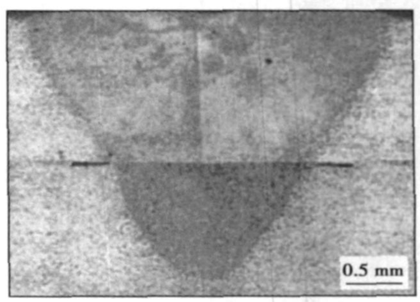


图 2 LF3Y2 铝合金试样焊接接头

Fig 2 Macrostructure of welded joint of aluminum alloy LF3Y2

## 2 有限元模型及其边界条件

### 2.1 控制方程

由热传导理论，固体传热现象可以用热传导微

收稿日期：2006－12－04
基金项目：国家自然科学基金资助项目（50575091）
*参加此项工作的还有张伟华

分方程和反映传热体和周围环境交互作用的边界条件来描述。热传导微分方程为

$$\rho c_{\mathrm{p}}(T)\frac{\partial T}{\partial t}=\frac{\partial}{\partial x}\left[\kappa(T)\frac{\partial T}{\partial x}\right]+\frac{\partial}{\partial y}\left[\kappa(T)\frac{\partial T}{\partial y}\right]+\frac{\partial}{\partial z}\left[\kappa(T)\frac{\partial T}{\partial z}\right]+Q(x,y,z,t)+H, \tag{1}$$

式中：$T$ 为温度；$t$ 为时间；$\rho$ 为密度；$\kappa$ 为导热系数；$c_{\mathrm{p}}$ 为材料定压比热容；$Q$ 为体热源热流密度；$H$ 为相变潜热。

### 2.2 热源模型

在激光深熔焊接模拟中，使用面热源模拟等离子体和表面熔池对工件的加热作用，采用体热源来模拟激光束挖掘作用导致的匙孔效应。在组合热源中，采用高斯型热流分布的面热源模型，对于体热源模型，由于激光束在匙孔内壁发生多重反射吸收，会产生能量衰减的现象，因此可以使用旋转高斯体热源模型。

高斯面热源模型为

$$q(x,y)=\frac{3Q}{\pi r_0^2}\exp\left[\frac{-3(x^2+y^2)}{r_0^2}\right], \tag{2}$$

式中：$r_0$ 为热源有效作用半径；$Q$ 为热源有效功率。

旋转高斯体热源模型为

$$q(x,y,z)=\frac{9P}{\pi R_0^2 H(1-\mathrm{e}^3)}\exp\left[\frac{-9}{\log\left(\frac{H}{z}\right)R_0^2}(x^2+y^2)\right], \tag{3}$$

式中：$H$ 为热源高度；$P$ 为热源有效功率；$R_0$ 为热源开口半径。

### 2.3 边界条件

首先考虑热流作用的高斯热流分布，工件表面上热流密度为已知，随位置和时间而变化。另外，分析中做以下假设。

(1) 不考虑工件与试验台之间的热传导。

(2) 忽略熔池内的金属流动，用体热源输入模型和等效热传导系数方法补偿对流，忽略熔池蒸发。

(3) 激光输出功率和材料对激光的吸收率不随时间变化。

(4) 除材料密度恒定不随时间变化外，其余热物理参数均随温度变化。

(5) 工件的初始温度为 400 ℃(RSW 提供)。

(6) 焊接以恒定速度进行。

(7) 由于 RSW 的热压作用，材料发生了塑性连接，搭接的二板无间隙，可视为一体。

由于激光焊接时工件和环境之间的温度差很大，它们之间产生对流换热，因此在上表面对流边界条件[7]为

$$-\lambda\frac{\partial T}{\partial z}=\begin{cases}q, & r\leqslant r_0;\\ h_{\mathrm{f}}(T-T_{\mathrm{a}}), & r>r_0。\end{cases} \tag{4}$$

式中：$h_{\mathrm{f}}$ 为换热系数；$q$ 为通过上表面吸收的热量；$r$ 为工件上表面任意一点到激光中心的距离。

在工件的其它表面，对流换热边界条件为

$$-\lambda\frac{\partial T}{\partial i}=h_{\mathrm{f}}(T-T_0),\quad i=x,y,z。 \tag{5}$$

## 3 数值计算及结果分析

### 3.1 热物理性参数和有限元网格划分

利用所建立的激光深熔焊有限元模型，对铝合金 LF3Y2 试件进行了数值计算，其热物理性参数见图 3。

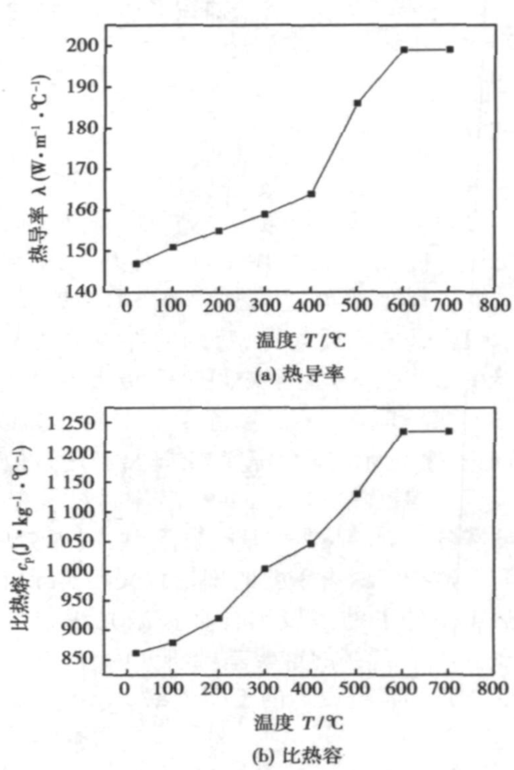


图 3 材料热物理性参数曲线

Fig. 3 Material thermal parameters curve

温度场模拟采用 ANSYS 通用有限元分析软件。为了减少网格数量，设工件沿焊缝截面对称，故取一半进行分析计算。建立有限元模型时，先建二维平面几何模型，采用过渡网格划分形式进行划分，使得距离焊缝大约 2 mm 宽的网格比较细密，而远离焊缝处的网格稀疏一些，然后由二维模型拉伸成三维模型。由于深熔焊接中激光束的直径非常小，所以将焊缝处的网格大小控制在 0.12～0.2 mm，网格划

分后的有限元模型如图 4 所示。

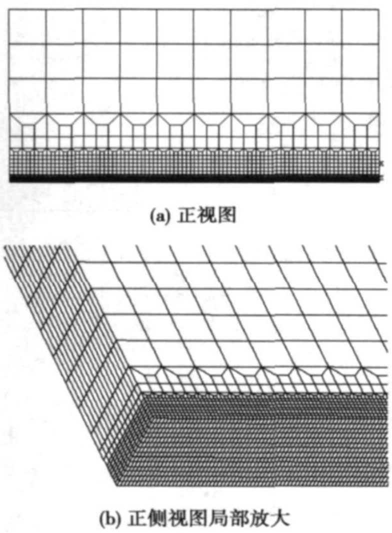


图 4　有限元网格

Fig. 4　Finite element mesh

## 3.2　模拟结果分析

从工艺上分析可知，由于热压对工件有预热缓冷的作用，改善了铝合金的焊接性，提高了工件表面对激光束的吸收率，增加了焊接热输入。图 5 和图 6 为热压条件下激光深熔焊接在 0.4 s 和 0.7 s 时的温度场分布。从图中可以看出热压使高速焊接时依然有很大的熔深和熔宽；熔池横截面上的温度场分布基本处于稳定状态；工件表面上的等温线成椭圆形，在移动热源前方等温线密集，温度梯度较大，移动热源后方等温线较稀疏，温度梯度小。

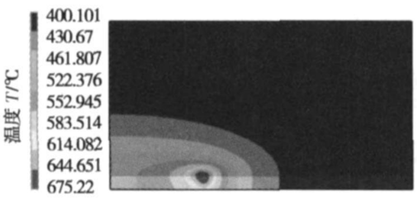


图 5　0.4 s 时温度场的模拟结果

Fig 5　Simulation result of temperature field in 0.4 seconds

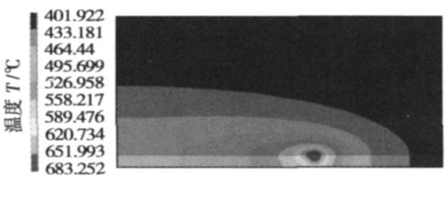


图 6　0.7 s 时温度场的模拟结果

Fig. 6　Simulation result of temperature field in 0.7 seconds

## 3.3　计算结果试验验证

图 7 为有限元模拟的熔池边界与实际焊缝熔合线的比较。从图中可以看出，模拟的焊接熔池边界处温度达到铝合金熔化温度以上，且其形貌与焊缝熔合线基本吻合，表明采用高斯面热源与旋转高斯体热源的组合热源形式模拟激光深熔焊接温度场是合理的。

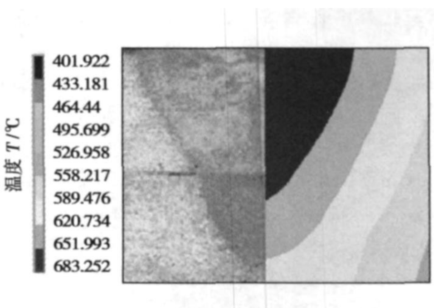


图 7　模拟熔池边界与焊缝熔合线对比

Fig 7　Contrast of simulation molten pool boundary and weld fusion line

# 4　结　　论

（1）通过工艺试验，对铝合金 LF3Y2 搭接板进行了热压条件下的激光深熔焊接，获得了焊接接头外观和金相照片。

（2）采用高斯面热源模拟等离子体和表面熔池对工件的加热作用，采用旋转高斯体热源模型来模拟匙孔对工件的加热作用，建立了复合热源模型。

（3）采用有限元分析的方法，对铝合金 LF3Y2 搭接板热压条件下的激光深熔焊接的热过程进行了数值模拟。同时，用模拟结果和工艺试验结果进行对比，证明采用面体组合热源模拟激光深熔焊接热过程是合理的热源模式。

参考文献：

[1]　左铁钏. 高强铝合金的激光加工[M]. 北京：国防工业出版社，2002.

[2]　赵熹华. 焊接方法与机电一体化[M]. 北京：机械工业出版社，2001.

[3]　Eibl M，Sonsino C M，Kaufmann H，*et al*. Fatigue assessment of laser welded thin sheet aluminium[J]. International Journal of Fatigue，2003，25(8)：719－731.

[4]　Haboudou A，Peyre P，Vannes A B，*et al*. Reduction of porosity content generated during Nd：YAG laser welding of A356 and AA5083 a-

luminium alloys[ J] . Materials Science and Engineering A, 2003, 363 (1—2): 40— 52.

[ 5] Palanco S, Klassen M, Skupin J, *et al*. Spectroscopic diagnostics on CW— laser welding plasmas of aluminum alloys[ C] // 1st International Conference on Laser Induced Plasma Spectroscopy and Applications. Elsevier Science B V, 2001: 651— 659.

[ 6] 赵熹华, 曹海鹏, 赵 贺. 激光束—电阻缝焊复合焊接方法基础研究[ C] // 第十一次全国焊接会议论文集. 哈尔滨: 黑龙江人民出版社, 2005: 388— 390.

[ 7] 杜汉斌, 胡伦骥, 王东川. 激光穿透焊温度场及流动场的数值模拟[ J] . 焊接学报, 2005, 26(12): 65— 68.

作者简介: 熊智军, 男, 1981 年出生, 硕士研究生。主要研究方向为焊接方法与机电一体化。

Email: bearxzj _yuan@sina.com

[ 上接第 36 页]

[ 8] 刘汉城, 汪正平, 李宁成, 等. 电子制造技术[ M] . 姜岩峰, 张常年, 译. 北京: 化学工业出版社, 2005.

[ 9] Kitajima M, Shono T. Development of Sn—Zn—Al lead-free solder alloys[ J] . Fujitsu Scientific and Technical Journal, 2005, 41(2): 225—235.

[ 10] Zhang Yue, Liang Tongxiang, Jusheng M A. Phase diagram calculation on Sn— Zn— Ga solders[ J] . Journal of Non-Crystalline Solids, 2004, 336(2): 153— 156.

[ 11] 张启运, 刘淑琪, 刘东升, 等. 微量添加元素对熔态 Sn—Pb 共晶合金抗氧化能力的影响[ J] . 金属学报, 1984, 20(4): A296— A302.

作者简介: 王 慧, 男, 1982 年出生, 博士研究生。主要从事微电子焊接技术及无铅钎料研究工作。发表论文 2 篇。

Email: huiwang@nuaa.edu.cn

tability of Sn—9Zn—X can be obviously improved in $N_2$ atmospheres. It is also found that Sn—9Zn—X lead-free solders show preferable wettability with $ZnCl_2$—$NH_4Cl$ flux, even better than that of Sn—3.5Ag—0.5Cu solder under the same condition, which may reveal the feasibility of improving the wettability of Sn—Zn series lead-free solders by developing suitable flux.

**Key words:** lead-free solder; Sn—Zn solder; alloy element; wettability

**Welding characteristics of laser-low power pulse MIG hybrid welding aluminium alloy** WANG Wei, WANG XuYou, QI GuoLiang, LEI Zhen, LIN ShangYang, DU Bing (Harbin Welding Institute, Harbin 150080, China). p37—40, 61

**Abstract:** The weld penetration, formation of weld, welding speed and weld heat input of MIG (metal inert-gas) welding and laser-MIG hybrid welding are analyzed for welding 5A06 aluminum alloy. It is shown that comparing with MIG welding, laser-MIG hybrid welding will increase depth-to-width ratio 100%—200% and increase weld penetration 43%—250%, as average current is less than 200 A and welding heat input and welding speed are equal. If welding heat input and average welding current are equal, welding speed of laser-MIG hybrid welding is higher 0.6—1.5 times than that of MIG welding, and weld penetration of laser-MIG hybrid welding is deeper 1.5—6.9 times than that of MIG welding. Equal weld penetration of laser-MIG hybrid welding and MIG welding can be obtained if lower welding heat input is applied in the hybrid welding and welding speed of the hybrid welding is 0.6—6.5 times higher than the one of MIG welding. Laser-MIG hybrid welding has good weld spreadability and is fit for high speed welding. It also was found that 2 kW laser power compounding with MIG will increase average arc voltage and decrease average welding current of MIG welding.

**Key words:** hybrid welding; laser welding; MIG welding; aluminum alloy welding

**Numerical simulation of temperature field in deep penetration laser welding under hot and press condition** XIONG Zhijun, LI Yongqiang, ZHAO Xihua, LI Min, ZHANG Weihua (School of Materials Science and Engineering, Jilin University, Changchun 130022, China). p41—44

**Abstract:** Deep penetration laser welding was performed at aluminum alloy LF3Y2 under hot and press condition. A heat source model, which comprises a gauss plane heat source on the top surface and a revolved gauss body heat source, was presented in this condition. Numerical simulation was adopted by the heat source model and ANSYS software. The results show that sufficient width and penetration of weld could be obtained under high speed welding operation and the isotherms looked like ellipse. The temperature gradient was correspondingly higher in the front of moving heat source than at the end. The cross-section morphology of simulation welded joint was almost in accordance with the results attained by experiments which confirmed the reasonableness of the model.

**Key words:** deep penetration laser welding; heat source model; numerical simulation; temperature field

**Effect of magnetic field on microstructure and properties of carbon arc surfacing layer** LIU Zhengjun, ZHANG Guiqing, YIN Yijun, ZENG Xiebo (School of Material Science and Engineering, Shenyang University of Technology, Shenyang 110023, China). p45—48

**Abstract:** In order to refine the structure of deposited metal and control the morphology and distribution of hard phases in surfacing deposited metal, DC transverse magnetic field was applied to the carbon arc surfacing of Cr—B—Ni—V iron based alloy system. The influence of magnetic intensity on hardness and wearing resistance was obtained through analyzing the hardness, wearing and microstructures of the surfacing deposited metal. The results show that the surfacing deposited metal of introducing magnetic field has higher hardness and better wearing resistance than the surfacing deposited metal without magnetic field; the properties of surfacing deposited metal are optimal when magnetic field current is 3 A, and surfacing current is 180 A, and surfacing speed is 12 cm/min. The hard phase in the surfacing deposited metal is fine and even, hexagonal in shape. Meanwhile the orientation of them is consistent.

**Key words:** transverse magnetic field; hardfacing; grinding abrasion; hard phase

**Mechanical properties of ring nugget in sheet-to-tube joining** LIANG Caiping, ZHANG Yansong, LAI Xinmin, CHEN Guanlong (School of Mechanical Engineering, Shanghai Jiao tong University, Shanghai 200030, China). p49—53

**Abstract:** Strength of resistance spot weld is determined by the physical attributes of weldment including material and geometric issues. The strength of the ring nugget in sheet-to-tube single-sided spot welding is different from that of the button nugget in traditional sheet-to-sheet spot welding. And the relationships between strength and attributes of ring nugget are unknown. Meanwhile, the large number of variables and experimental uncertainty also make it difficult to establish this relationships. A numerical simulation experiment was conducted using the concept of design of experiments (DOE) and the method of finite element based on the tensile-shear tests. The mechanical properties during tensile-shear process was analyzed and quantitative relationships were established to link a weld's tensile-shear force and its geometrical attributes, which supplied the proof for the nugget quality estimation.

**Key words:** single-sided spot welding; numerical simulation; ring nugget; mechanical properties

**Extraction of welding pool shape using linear approximation** WANG Jifeng, WANG Wenyi, CHEN Shanben (Institute. of Welding Technology, Shanghai Jiaotong University, Shanghai 200030, China). p54—56

**Abstract:** The welding bead shape is crucial for welding quality. Three-dimensional shape of the welding pool contain much information about quality. Thus, shape from shading technique was